2011

Role of Hydrodynamic Behavior of DNA Molecules in Dielectrophoretic Polarization Under the Action of an Electric Field

Hui Zhao
University of Nevada, Las Vegas, hui.zhao@unlv.edu

Role of hydrodynamic behavior of DNA molecules in dielectrophoretic polarization under the action of an electric field

Hui Zhao*

Department of Mechanical Engineering, University of Nevada Las Vegas, Las Vegas, Nevada 89154, USA

(Received 11 April 2011; revised manuscript received 23 June 2011; published 8 August 2011)

A continuum model is developed to predict the dielectrophoretic polarizability of coiled DNA molecules under the action of an alternating current electric field. The model approximates the coiled DNA molecule as a charged porous spherical particle. The model explains the discrepancies among scaling laws of polarizability of different-sized DNA molecules with contour length and such discrepancies are attributed to different hydrodynamic behavior. With zero or one fitting parameter, theoretical predictions are in good agreement with various experimental data, even though in experiments there are some uncertainties in regard to certain parameters.

DOI: 10.1103/PhysRevE.84.021910 PACS number(s): 87.14.gk, 82.45.Tv, 47.65.−d

I. INTRODUCTION

Dielectrophoresis (DEP) has been proposed to assemble DNA molecules into molecular electronics, which holds the promise of revolutionizing semiconductor manufacturing [1]. In addition, DEP is also widely used to manipulate DNA molecules including trapping [2,3], immobilization [4,5], separation, and purification [6,7], with applications to biotechnology and nanotechnology.

To optimize the usage of DEP in the aforementioned applications, it is important to understand the physical properties of DNA, particularly its dielectrophoretic polarization, which determines its interaction with external electric fields. Considerable experimental studies have been conducted to characterize the polarizability [1]. For example, its dependencies on contour length, electric field frequency, and bulk concentration have been intensively examined by various methods, i.e., transient electric birefringence [8,9], dielectric spectroscopy [10,11], and optical microscope observing the escape of DNA from DEP traps [5–7]. Scaling laws of measured polarizabilities (α) with the number of base pairs (N) ($\alpha \sim N^{\beta}$) exhibit a wide range of scatter: for linear DNA molecules, Stellwagen [8] found $\beta = 2$ when N is less than 300 base pairs (bp). Elias and Eden [9] reported $\beta = 3$ in a range up to 120 bp and gradually changed to a linear relation ($\beta = 1$) when N ranges from 300 bp to 5 kbp. For N from 6 to 164 kbp, β was fitted to be 0.4 ± 0.1 [6,7]. For supercoiled DNA molecules ranging from 7 to 21 kbp, $\beta = 2.0 \pm 0.4$ [7]. The discrepancies among β values of different-sized DNA molecules indicate that a coherent systematic study of the underlying physics governing the polarization is in need.

Compared to considerable efforts made in experimental investigations, theoretical understanding of polarization of a DNA molecule attracts less attention. Most theoretical studies are mainly based on the Maxwell-Wagner model relying on empirical parameters fitted by experimental data. However, even with fitting parameters, the Maxwell-Wagner model still cannot fully explain the frequency dependance of the polarizability and fails to predict the low-frequency dispersion without making further assumptions. On the other hand, the Poisson-Nernst-Planck equations coupled with the Stokes equation have been demonstrated to be capable of predicting the polarization of rigid particles over a broad range of frequency (termed the PNP model) [12]. When the contour length of a DNA molecule is less than its persistence length (∼150 bp) [13], the DNA can be modeled as a rigid elongated rod and theoretical predictions from the PNP model without any fitting parameters were compared and favorably agreed with experimental data for double stranded, short DNA molecules ($N < 150$ bp) [14]. In addition, theoretical predictions are qualitatively consistent with experimental observations that reported superlinear dependence of the polarizability on the contour length for shorter molecules [9]. However, the above PNP model is not applicable for long DNA molecules as these molecules are likely to bend and coil.

II. MATHEMATICAL MODEL

In this paper, we modify the standard PNP model to accommodate the configuration of a long and coiled DNA molecule. As a first step, we approximate a coiled DNA molecule as a charged porous spherical particle with a radius R_g where R_g is the radius of gyration [15,16]. For linear DNA molecules, R_g is given by [17]

$$R_g = L_a\left[\frac{L}{3L_a} - 1 + \frac{2L_a}{L} - 2\left(\frac{L_a}{L}\right)^2(1 - e^{-L/L_a})\right]^{1/2}. \quad (1)$$

In the above, L is the DNA contour length, which is equal to the product of the number of base pairs (N) and the axial distance per base pair (0.34 nm) and $L_a = 46$ nm is a fitting parameter. Equation (1) was in good agreement with experimental data for linear DNA molecules [17].

The spherical porous particle is assumed to have uniformly distributed fixed electric charge density within the entire sphere. The electric charge attracts counterions, repels coions, and forms an electric double layer (EDL) within and near the porous sphere. A uniform ac electric field ($E_0 e^{i\omega t}\vec{e}_z$) imposes an electrostatic force on mobile ions in the solution. Excess counterions inside the EDL migrate, drag water with them, and induce an electro-omostic flow. Simultaneously, the charged porous sphere experiences an electrophoretic motion with

*hui.zhao@unlv.edu

a velocity $\vec{U}(t) = U_0 e^{i\omega t}$ which also drags the surrounding liquid to move. To facilitate the computation, we use the Galilean transformation to fix the origin of the coordinate system at the particle's center. The particle's velocity $\vec{U}$ is not known *a priori* and will be determined as part of the solution process. We use the spherical coordinate system (r,θ,φ) with its origin at the center of the particle. θ is defined as the angle between $\vec{e}_z$ and $\vec{e}_r$.

For simplification, here we will focus on a 1-1 binary electrolyte with permittivity ϵ (it is straightforward to adapt to a general electrolyte). Since the Reynolds number associated with electrokinetic flows is small, the flow velocities $\vec{u}$ satisfy the Stokes equation:

$$-\nabla p + \mu\nabla^2\vec{u} - \rho\nabla\phi - h(r)\gamma\vec{u} = 0. \tag{2}$$

The fluid is incompressible:

$$\nabla\cdot\vec{u} = 0. \tag{3}$$

The electric potential ϕ obeys the Poisson equation

$$\epsilon\nabla^2\phi = -(\rho + h(r)\rho_{\rm fix}). \tag{4}$$

Ionic concentrations $(C_\pm)$ are governed by the Nernst-Planck equations,

$$\frac{\partial C_\pm}{\partial t} = \nabla\cdot\left[D_\pm\nabla C_\pm + \frac{F_a D_\pm z_\pm}{RT}C_\pm\nabla\phi - C_\pm\vec{u}\right]. \tag{5}$$

In the above, $\rho = F_a(C_+ - C_-)$ is the charge density due to mobile ions; F_a is the Faraday constant; $z_\pm = \pm 1$ is ions' valence; $\rho_{\rm fix} = \rho_0 N/V_p$ is the fixed charge density of the porous sphere where $V_p = 4/3\pi R_g^3$ is the volume occupied by the DNA and $\rho_0 = 0.33\times 10^{-18} C/{\rm bp}$ is the DNA linear charge density [1]. $h(r)$ is a function of location: $h(r) = 1$ for the region occupied by a DNA ($r \leqslant R_g$) and $h(r) = 0$ for the rest ($r > R_g$). $\gamma = \mu f N_s$ is the hydrodynamic frictional coefficient inside the porous sphere. $N_s = N/(150V_p)$ is the number density of the hydrodynamic frictional polymer segments; since DNA can be viewed as a connection of rigid segments, each segment can be considered as a rod with a radius of $a = 1$ nm and a length of its persistence length $L_p = 50$ nm (150 bp) [18,19], and there are $N/150$ segments in total. f is the draining factor.

Far from the particle,

$$\begin{aligned}&\phi = E_0 r\cos\theta e^{i\omega t}, \quad C_\pm = C_0, \quad \text{and}\\ &\vec{u} = -U_0 e^{i\omega t}\vec{e}_z \quad \text{at } r\to\infty.\end{aligned} \tag{6}$$

It is recognized that similar equations to Eqs. (2)–(5) were also used to model soft particles [20–22].

Assuming that the imposed electric field is much smaller than that induced by the fixed charge, one can use a regular perturbation expansion in terms of the applied electric field about the fix charge:

$$\begin{pmatrix}\phi\\ C_\pm\\ \vec{u}\end{pmatrix} = \begin{pmatrix}\phi^{(0)}\\ C_\pm^{(0)}\\ 0\end{pmatrix} + \delta{\rm Re}\left[\begin{pmatrix}\phi^{(1)}\\ C_\pm^{(1)}\\ \vec{u}^{(1)}\end{pmatrix}e^{i\omega t}\right] + O(\delta^2), \tag{7}$$

where the symbol Re is the real part of a complex number and δ is the ratio between the magnitude of the external electric field and that associated with the fix charge.

A. Zeroth order approximation

In the absence of an external electric field, there is no flow and the ions' concentrations obey the Boltzmann distribution:

$$C_\pm^{(0)} = C_0 e^{\mp F_a\phi^{(0)}/RT}. \tag{8}$$

The electric potential $\phi^{(0)}$ satisfies

$$\epsilon\nabla^2\phi^{(0)} = 2F_a C_0\sinh\left(\frac{F_a\phi^{(0)}}{RT}\right) - h(r)\rho_{\rm fix}. \tag{9}$$

The boundary conditions are

$$\phi^{(0)}(0) = \frac{RT}{F_a}{\rm asinh}\left(\frac{\rho_{\rm fix}}{2F_a C_0}\right) \quad \text{and} \quad \phi^{(0)}(\infty) = 0. \tag{10}$$

B. First-order approximation

The first-order equations are linear in the perturbed quantities and the dependent variables oscillate at the forcing frequency. Accounting for the linearity of the first-order equations, one can decompose the first-order problem into two problems: (1) the **E** problem consists of a stationary sphere under the action of the same electric field as the original problem at infinity, and (2) the **U** problem consists of a stationary sphere in a uniform flow field in the absence of the external electric field [12,23–25]. Once the solutions of **E** and **U** are obtained, the solutions of the first-order problem can be written as the superposition:

$$X^{(1)} = (X^{(1)E} + U_0 X^{(1)U})e^{i\omega t}, \tag{11}$$

where U_0 is the electrophoretic mobility and will be determined by nullifying the net force acting on the particle.

All the equations are identical for **E** and **U** problems. We omit below the superscripts **E** and **U**. Substituting Eq. (7) into Eqs. (2)–(5), retaining terms up to the first order, and replacing the time derivative with $i\omega$, we have

$$-\nabla p^{(1)} + \mu\nabla^2\vec{u}^{(1)} - \rho^{(0)}\nabla\phi^{(1)} - \rho^{(1)}\nabla\phi^{(0)} - h(r)\gamma\vec{u}^{(1)} = 0, \tag{12}$$

$$\nabla\cdot\vec{u}^{(1)} = 0, \tag{13}$$

$$\epsilon\nabla^2\phi^{(1)} = -\rho^{(1)}, \tag{14}$$

$$i\omega C_\pm^{(1)} = \nabla\cdot\left[D_\pm\nabla C_\pm^{(1)} + \frac{F_a D_\pm z_\pm}{RT}(C_\pm^{(0)}\nabla\phi^{(1)} + C_\pm^{(1)}\nabla\phi^{(0)}) - C_\pm^{(0)}\vec{u}^{(1)}\right]. \tag{15}$$

III. SOLUTION PROCEDURE AND CODE VERIFICATION

The above zeroth-order and first-order equations with corresponding boundary conditions were solved by the commercial finite element software COMSOL 3.5 (Comsol, Los Angeles, USA). The computational domain consisted of a finite domain $0 \leqslant r \leqslant R$. We selected $R = 10^4$ since a tenfold increase in R resulted in variations smaller than 1%, indicating that the domain is sufficiently large to render the computational results R independent. To resolve the details of the electric double

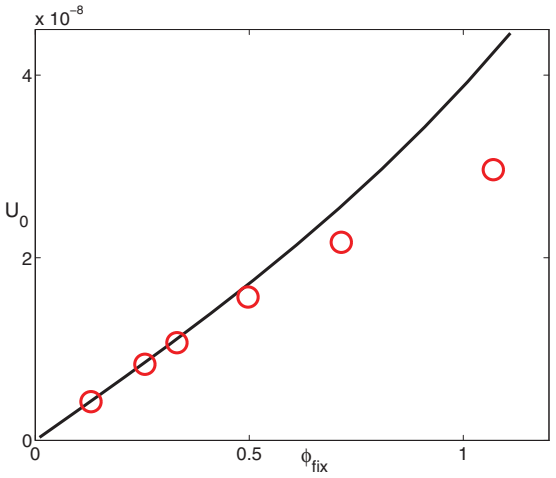

FIG. 1. (Color online) The electrophoretic mobility U_0 as a function of dimensionless Donnan potential when $\kappa R_g = 50$ and $\lambda R_g = 40$. The line and the symbols correspond, respectively, to the mobility predicted by Eq. (16) and that computed by numerical simulations.

layer and porous particle, nonuniform elements were used with a dense mesh concentrated inside the particle and next to the particle surface as well. The element size gradually increases as the distance from the particle increases. The mesh was refined a few times to make sure that the results are mesh independent.

To verify the computational algorithm, we computed the electrophoretic mobility of a porous particle in the case of thin double layers and compared our numerical results with the analytical solution [15,26]:

$$U_0 = \frac{\rho_{\text{fix}}}{\mu\lambda^2}\left[1 + \frac{1}{3}\left(\frac{\lambda}{\kappa}\right)^2 \frac{2\kappa + \lambda}{\kappa + \lambda}\right], \tag{16}$$

where $\lambda = \sqrt{\gamma/\mu}$ and $\kappa = \sqrt{2F_a^2 C_0/\epsilon RT}$ is the inverse of Debye screening length. Equation (16) was derived under the assumption of $\kappa R_g \ll 1$ and $\lambda R_g \ll 1$ [15,26].

Figure 1 plots the mobility U_0 as a function of the dimensionless Donnan potential $\phi_{\text{fix}} = \text{asinh}(\frac{\rho_{\text{fix}}}{2F_a C_0})$ normalized by RT/F_a when $\kappa R_g = 50$ and $\lambda R_g = 40$. The line and the symbols correspond, respectively, to the mobility predicted by Eq. (16) and that computed by numerical simulations. Our numerical simulations agreed well with Eq. (16) when $\phi_{\text{fix}} < 1$. Since Eq. (16) is derived under the condition of low Donnan potentials by neglecting double layer polarization [16,26], it is not surprising that the computed mobility deviates from theoretical prediction at large ϕ_{fix}.

IV. RESULTS

The DNA and its adjacent EDL perturb the electric field. Far from the DNA, the first-order perturbed field behaves like a field induced by a dipole and the electric potential admits the form $E_0 \cos\theta(-r + K/r^2)$, where K is the dipole moment and can be deduced from the behavior of the first-order electric potential as a function of r sufficiently far from the particle ($0 \ll r \ll R$). The DNA polarizability α is $2\pi\epsilon\text{Re}(K)$.

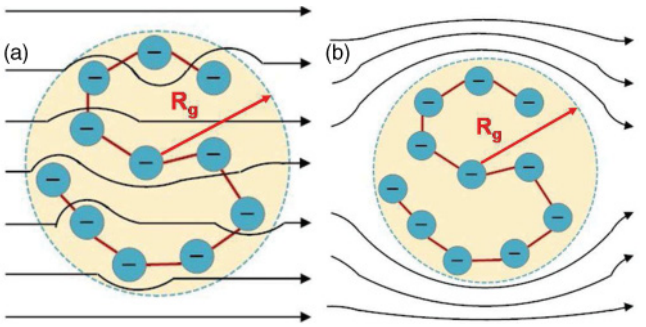

FIG. 2. (Color online) A schematic of draining conditions: (a) free draining; (b) nondraining.

In our continuum model (2)–(5), only the draining factor f is unknown *a priori* and all remaining parameters are fixed for a given DNA. f depends on the hydrodynamic behavior of a DNA [15] and the hydrodynamic behavior of a DNA is affected by degree of draining [27].

Draining can be categorized into three types: (1) free draining; (2) partial draining; (3) nondraining. Free draining implies that the perturbation to the flow field induced by one polymer segment has no impact on the flow fields near other polymer segments. In other words, the fluid appears to penetrate the DNA and interacts with each segment independently [Fig. 2(a)]. In this case, the draining factor $f = 4\pi L_p/[\ln(L_p/a) + 0.193]$ (153 nm) for a rod-shaped segment with a radius of $a = 1$ nm and a length of $L_p = 50$ nm [28]. For larger polymers, the free-draining condition appears to break down [27]. Instead, partial-draining condition was proposed to explain the experimental observations where neighboring polymer segments partially screen more interior units from the flow [29]. Under the partial-draining condition, the draining factor f is believed to be larger than that of free draining. In the limit of the strong screening, often termed nondraining, condition ($f \to \infty$), the flow cannot penetrate into the DNA and the DNA acts like an impermeable sphere with a radius of R_g [Fig. 2(b)]. Hence f ranges from 153 nm to ∞. Here we must emphasize that in the case of nondraining, although there is no flow inside the DNA, mobile ions still can migrate into/out of the DNA and such migration can influence the polarizability.

It is recognized that the larger the draining factor (f), the smaller the polarizability (α) since a larger draining factor corresponds to weaker convection inside the porous sphere, which leads to a reduction of α. However, how f affects scaling laws of α with contour length remains unknown and is worthstudying.

In the set of experiments, Elias and Eden [9] deduced electrical polarizability of linear DNA molecules ranging from 64 bp to 5 kbp in 1 mM Na^+ solution via transient electric birefringence at 4 °C and around the kHz frequency range. Here we only focus on DNA molecules whose contour length is larger than their persistence length. Thus we can treat the DNA as a porous sphere. Figure 2(a) depicts the polarizability α as a function of N. In our simulations, R_g is given by Eq. (1). With respect to free draining and nondraining (solid and dash-dotted lines), there are no fitting parameters. In the case of partial draining (dashed line), the draining factor ($f = 1000$ nm) was

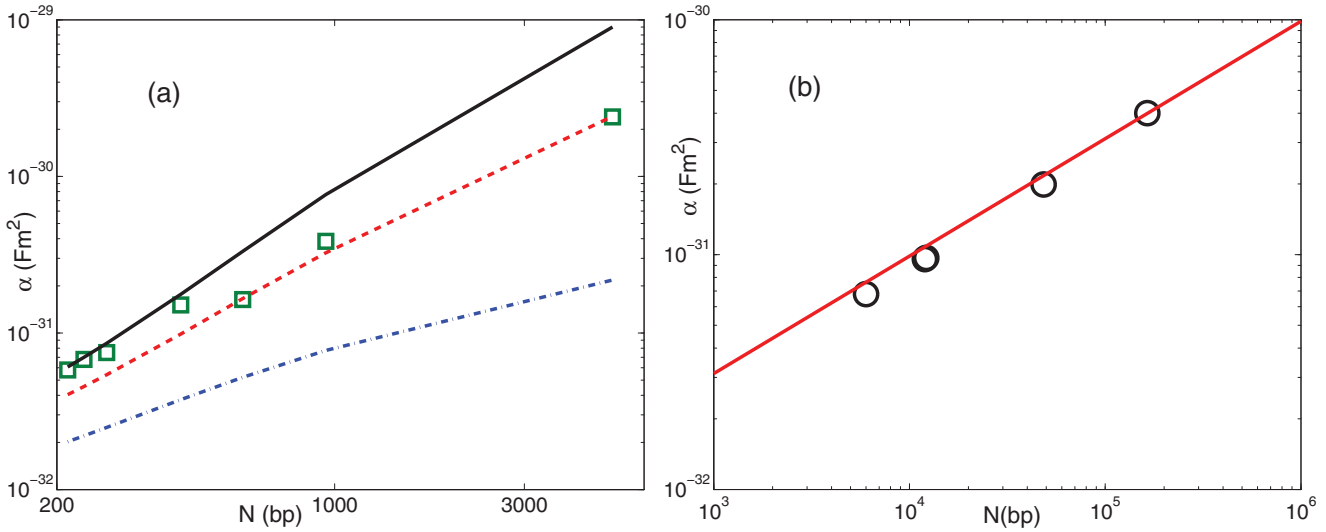

FIG. 3. (Color online) The polarizability α (Fm^2) as a function of N. (a) For DNA molecules ranging from 200 bp to 5 kbp, the symbols correspond to experimental data [9]. The solid, dashed, and dash-dotted lines correspond, respectively, to the theoretical predications of free draining ($f = 153$ nm), partial draining ($f = 1000$ nm), and nondraining ($f \to \infty$). (b) For DNA molecules from 6 kbp to 164 kbp [7], symbols correspond to theoretical predictions of nondraining ($f \to \infty$). The line is fitted to reveal a scaling relation $\alpha \sim N^{\beta}$.

fitted by matching the polarizability of 5 kbp DNA and the rest of the parameters remain the same as those in the experiment. Figure 3(a) strongly suggests that different-sized DNA molecules adopt different draining conditions and have distinct hydrodynamic behavior: When $N < 500$ bp, DNA moves in the form of free draining. As N increases ($N > 500$ bp), partial draining becomes more appropriate to describe the hydrodynamics. The different hydrodynamic behavior can be explained: there are experimental evidences that in the presence of an external electric field, long DNA molecules are more likely to be stretched [30,31]. Thus, owing to stretching, the persistence length may increase and interactions among polymer segments may become appreciable. Both effects can contribute to an increase of the draining factor f.

For even longer linear DNA molecules ranging from 6 to 164 kbp, a different scaling law ($\alpha \sim N^{0.4\pm0.1}$) was reported in contrast to the linear relation ($\alpha \sim N$) held by DNA molecules below 5 kbp [7]. Figure 3(b) plots theoretically predicted α as a function of N ($N \geqslant 6$ kbp) in a 2 mM Na^+ solution at 60 Hz where parameters except f are the same as those reported in experiments [7]. Symbols are theoretical predictions in the case of nondraining. The line is best fitted to reveal scaling laws ($\alpha \sim N^{\beta}$) where $\beta = 0.5$, which is consistent with the experiment [7]. In contrast to Fig. 3(a) where good quantitative agreements with experiments were observed, Fig. 3(b) indicates that our model underestimates α by orders of magnitude compared to experimental data where α is around 10^{-29} Fm^2. Nonetheless, still, our model accurately captures the scaling law and suggests that very long coiled DNA molecules ($N \geqslant 6$ kbp) act more like nondraining entities. It is recognized that for large N, the excluded-volume effect, where a position in space cannot be occupied by two segments at the same time, can induce an extra repulsion. In other words, the conformation of very long DNA ($N \geqslant 6$ kbp) is no longer a Gaussian coil as that of short DNA [18]. The crossover N from random coil to excluded-volume conformation is about 10 kbp depending on salt concentration [32,33]. One shall expect that this excluded-volume effect may further increase f due to extra repulsion, giving rise to the nondraining condition for very long DNA molecules.

To further conform our speculation, we compare our theoretical predictions to another set of experiments. In Fig. 4, α is plotted against the frequency ω for a 12 kbp linear DNA in ddH_2O without any fitting parameters. Figure 4 suggests that theoretical predictions with nondraining agree much better with experimental data than those with free draining. The polarizability of partial draining lies in between those of free

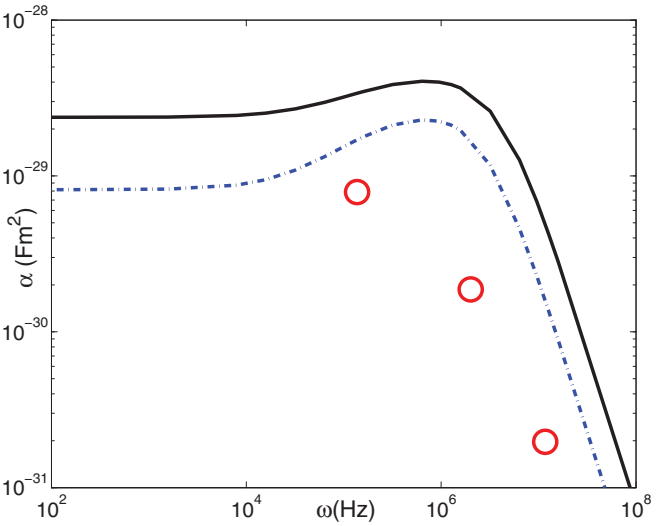

FIG. 4. (Color online) The polarizability α (Fm^2) as a function of the frequency ω for a 12 kbp linear DNA molecule. The symbols correspond to experimental data [10]. The solid and dash-dotted lines correspond, respectively, to the theoretical predications of free draining ($f = 153$ nm), and nondraining ($f \to \infty$).

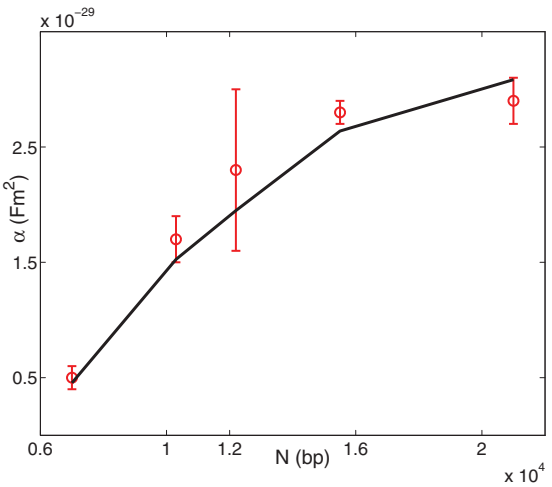

FIG. 5. (Color online) The polarizability α (Fm^2) of supercoiled DNA molecules as a function of N. The symbols and the line correspond, respectively, to experimental data [7] and theoretical predictions of free draining ($f = 153$ nm).

draining and nondraining (not shown here). In other words, the comparisons with a different set of experiments conform to our assumption that the excluded-volume conformation adopted by very long linear DNA molecules ($N \geqslant 6$ kbp) possibly shields flow away from the DNA and the DNA behaves like an impermeable sphere [Fig. 2(b)].

In summary, for linear DNA, the hydrodynamic behavior of DNA plays an important role in determining the polarizability. It changes from free draining to partial draining and eventually reaches nondraining as the contour length of N increases. It is different hydrodynamic behavior adopted by different-sized DNA molecules resulting in scattered scaling laws.

Finally, we turn our attention to supercoiled DNA molecules where the situation is quite different. Supercoiled DNA molecules often have a branched plectonemic structure (a starlike configuration) rather than random coiled one adopted by their linear counterparts [7,34]. Such unique spatial conformation is expected to impact the hydrodynamic behavior and hence modifies the polarization. Indeed, Regtmeier *et al.* [7] measured the polarizability of supercoiled DNA molecules ranging from 7 to 21 kbp and discovered that their polarization is qualitatively different from that of linear DNA molecules. Here we apply our model to study the polarization of supercoiled DNA molecules. In our model, parameters are the same as those of linear DNA molecules except that the radius of gyration (R_g) is obtained from experimental measurements [7].

Figure 5 compared our theoretical predictions assuming that supercoiled DNA molecules adopt free draining with experimental data. In Fig. 5 there are no fitting parameters. The agreements are remarkable. Not only does our model capture the scaling law of the polarizability with N, but also theoretical predictions quantitatively agree well with experiments. The excellent agreements strongly suggest that the hydrodynamic behavior of supercoiled DNA molecules has the form of free draining. The configuration of supercoiled DNA is starlike with visible branches as shown by AFM (Fig. 6 in [7]) and this loose structure may effectively reduce the impact of the excluded-volume effect on hydrodynamic interactions among segments. Hence it is possible that each segment becomes hydrodynamically independent again.

V. CONCLUSION

In summary, we developed a continuum model to quantitatively characterize the dielectrophoretic polarization of DNA molecules. Our predicted polarizabilities of both linear and supercoiled DNA molecules were in reasonable agreement with various experimental data with zero or only one fitting parameter. More importantly, our model suggested that the different hydrodynamic behavior adopted by different-sized DNA molecules is responsible for the discrepancies among scaling laws of polarizability with contour length. Our continuum model is not restricted to DEP only and can be readily extended to study other electrokinetic phenomena associated with coiled DNA molecules, such as electrophoresis.

ACKNOWLEDGMENT

This work was supported, in part, by UNLV URBAN 21 Innovation Grant.

[1] R. Holzel, IET Nanobiotechnol. **3**, 28 (2009).
[2] C. Asbury, A. Diercks, and G. Engh, Electrophoresis **23**, 2658 (2002).
[3] C. Chou, J. Tegenfeldt, O. Bakajin, S. Chan, E. Cox, N. Darnton, T. Duke, and R. Austin, Biophys. J. **83**, 2170 (2002).
[4] M. Washizu, O. Kurosawa, I. Arai, S. Suzuki, and N. Shimamoto, IEEE Tran. Ind. Appl. **31**, 447 (1995).
[5] S. Tuukkanen, A. Kuzyk, J. Toppari, H. Hakkinen, V. Hytonen, E. Niskanen, M. Rinkio, and P. Torma, Nanotechnology **18**, 295204 (2007).
[6] J. Regtmeier, T. T. Duong, R. Eichhorn, D. Anselmetti, and A. Ros, Anal. Chem. **79**, 3925 (2007).
[7] J. Regtmeier, R. Eichhorn, L. Bogunovic, A. Ros, and D. Anselmetti, Anal. Chem. **82**, 7141 (2010).
[8] N. C. Stellwagen, Biopolymers **20**, 399 (1981).
[9] J. Elias and D. Eden, Macromolecules **14**, 410 (1981).
[10] D. Bakewell, I. Ermolina, H. Morgan, J. Milner, and Y. Feldman, Biochim. Biophys. Acta **1493**, 151 (2000).
[11] S. Omori, Y. Katsumoto, A. Yasuda, and K. Asami, Phys. Rev. E **73**, 050901 (2006).
[12] H. Zhao and H. H. Bau, J. Colloid Interface Sci. **333**, 663 (2009).
[13] C. Bouchiat, M. D. Wang, J. F. Allemand, T. Strick, S. M. Block, and V. Croquette, Biopolymers **20**, 1481 (1999).
[14] H. Zhao and H. H. Bau, Langmuir **26**, 5412 (2010).
[15] H. Ohshima, Adv. Colloid Interface Sci. **62**, 189 (1995).

[16] L. H. Yeh and J. P. Hsu, Soft Matter **7**, 396 (2010).
[17] D. R. Latulippe and A. L. Zydney, Biotechnol. Bioeng. **107**, 134 (2010).
[18] J. Viovy, Rev. Mod. Phys. **72**, 813 (2000).
[19] K. D. Dorfman, Rev. Mod. Phys. **82**, 2903 (2010).
[20] H. Ohshima, J. Colloid Interface Sci. **233**, 142 (2001).
[21] R. J. Hill, D. A. Saville, and W. B. Russel, J. Colloid Interface Sci. **263**, 478 (2003).
[22] J. J. Lopez-Garcia, C. Grosse, and J. J. Horno, J. Colloid Interface Sci. **265**, 341 (2003).
[23] R. W. O'Brien and L. R. White, J. Chem. Soc. Faraday Trans. **74**, 1607 (1978).
[24] H. Zhao, Phys. Fluids **7**, 072004 (2010).
[25] H. Zhao, J. Phys. Chem. C **18**, 8389 (2010).
[26] J. J. Hermans, J. Polymer Sci. **18**, 527 (1955).
[27] R. M. Peitzsch, M. J. Burt, and W. F. Reed, Macromolecules **25**, 806 (1992).
[28] R. Probstein, *Physicochemical Hydrodynamics* (Butterworths, Boston, 1989).
[29] P. Debye, Phys. Rev. **71**, 486 (1947).
[30] V. Namasivayam, R. G. Larson, D. T. Burke, and M. A. Burns, Anal. Chem. **74**, 3378 (2002).
[31] L. Lam, S. Sakakihara, K. Ishizuka, S. Takeuchi, and H. Noji, Lab Chip **7**, 1738 (2007).
[32] R. J. Douthart and V. Bloomfield, Biopolymers **6**, 1297 (1968).
[33] D. E. Smith, T. T. Perkins, and S. Chu, Macromolecules **29**, 1372 (1969).
[34] T. C. Boles, J. H. White, and N. R. Cozzarelli, J. Mol. Biol. **213**, 931 (1990).